Matter

CellPress
OPEN ACCESS

Article

Co-assembling living material as an *in vitro* lung epithelial infection model

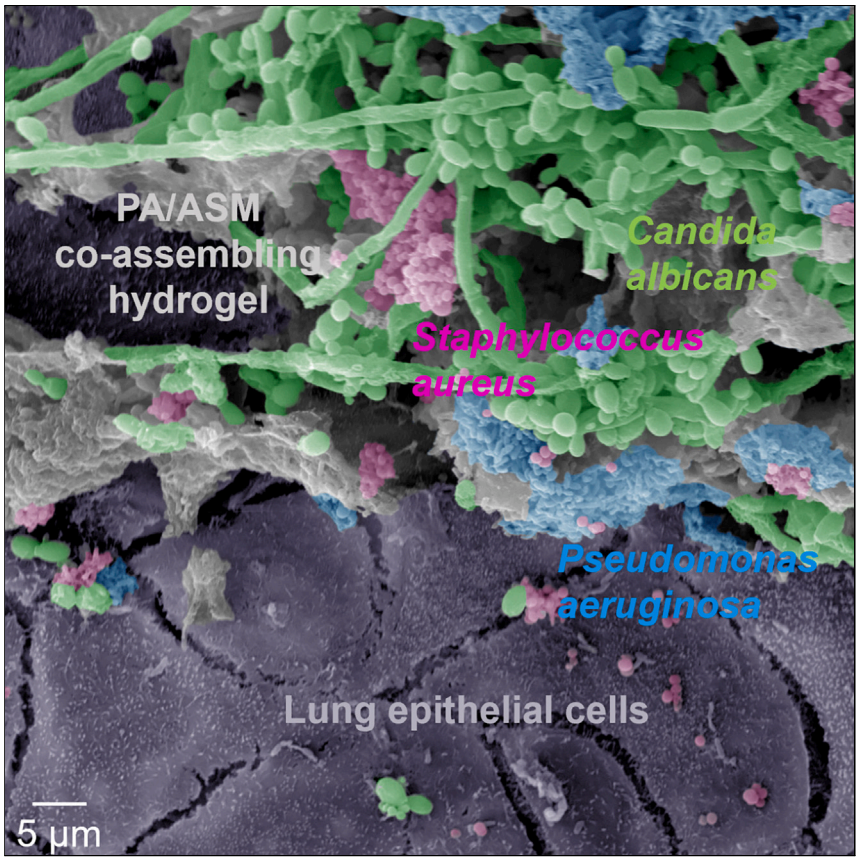

There is currently an unmet need to recreate 3D biofilms, which are the source of major hazards, such as contamination in hospitals and resistance to antibiotics. We design a self-organized material platform based on bacterial culture medium manipulated by peptide amphiphiles into hydrogels. This hydrogel can support the growth of 3D biofilms with nutritional elements and mechanical strength and enables co-culture with lung epithelial cells to serve as an *in vitro* model for estimating the impact of antibiotics.

Yuanhao Wu, Manuel Romero, Shaun N. Robertson, ..., Jiaming Sun, Miguel Cámara, Alvaro Mata

yuanhaowu@hust.edu.cn (Y.W.)
a.mata@nottingham.ac.uk (A.M.)

Highlights

PAs are used to signal bacteria and co-assemble with ASM into hydrogel

The PA-ASM hydrogel enables polymicrobial growth as living material for bioprinting

The living material can be co-cultured with lung epithelial cells in an *in vitro* model

Benchmark
First qualification/assessment of material properties and/or performance

Wu et al., Matter 7, 1–21
January 3, 2024 © 2023 The Authors. Published by Elsevier Inc.
https://doi.org/10.1016/j.matt.2023.10.029

Please cite this article in press as: Wu et al., Co-assembling living material as an *in vitro* lung epithelial infection model, Matter (2023), https://doi.org/10.1016/j.matt.2023.10.029

Matter

CellPress
OPEN ACCESS

Article

Co-assembling living material as an *in vitro* lung epithelial infection model

Yuanhao Wu,[1,2,3,4,13,*] Manuel Romero,[3,5,6,7,13] Shaun N. Robertson,[3,5,6] Samuel Fenn,[3,5,6,8] Leanne Fisher,[6] Iona Willingham,[3,5,6] Luisa Martinez Pomares,[6] Cosimo Ligorio,[3,4] Jordan Hill,[3,4,9] Wenhuan Bu,[3,4,10,11] Zuoxin Zhou,[9] Ricky D. Wildman,[9] Amir M. Ghaemmaghami,[6] Hongchen Sun,[10,11] Jiaming Sun,[1,2] Miguel Cámara,[3,5,6] and Alvaro Mata[3,4,9,12,14,*]

SUMMARY

Biofilms are robust living 3D materials that play key roles in nature but also cause major problems, such as tolerance to antibiotic treatment. Recreation of these living structures *in vitro* is critical to understand their biology and develop solutions to the problems they cause. However, growing 3D biofilms *in vitro* is difficult primarily because of the limitations in developing matrices that mimic the inherent structural and compositional complexity of their extracellular milieu. Here, we report a living material based on the co-assembly of artificial sputum medium with bioactive peptide amphiphiles. We demonstrate its capacity to support the growth of 3D polymicrobial biofilms and build an interkingdom infected lung epithelial model to study the impact of the antibiotic ciprofloxacin. Our study offers a living material capable of growing functional 3D biofilms that simulate *in vitro* the nutritional and mechanical properties of these systems *in vivo*.

INTRODUCTION

There is growing interest in living materials that have characteristics of living organisms, such as the ability to adapt, be autonomous, and display the capacity to grow.[1] These living materials consist of extracellular matrix materials (ECMMs) embedding living components, such as engineered cells and bacteria, which are able to modify the structure and properties of the ECMMs[2]. Particular attention is being paid to enhancing the integration of synthetic ECMMs with living components. Aiming to overcome this challenge, recent pioneering studies have reported ingestible polydimethylsiloxane bacterium-based biosensors to detect gastrointestinal bleeding in real time[3] and an F127-bisurethane methacrylate material comprising multiple engineered bacteria capable of programming the synthesis of hydrogels.[4] However, a major limitation continues to be the lack of materials that can recreate the inherent structural and compositional complexity of the natural living milieu.[5] Such materials would offer unique opportunities to enhance the functionality and impact of engineered living materials.[6]

Biofilms are natural living communities made of assemblages of microbial cells within 3D extracellular polymeric substances (EPSs) of self-produced high-molecular-weight biopolymers such as polysaccharides, extracellular DNA, proteins, and lipids.[7] Because of this special assembly, biofilms can dynamically adapt to environmental cues and produce EPSs, which make up to 50%–90% of the total organic material in the community and confer increased tolerance to antibiotics and

PROGRESS AND POTENTIAL

3D biofilms are the source of major hazards, such as contamination in hospitals and resistance to antibiotics. There is an unmet need to create 3D biofilms *in vitro* to understand their biology and develop solutions to the problems they cause. Here, we report a living material platform made by co-assembly of artificial sputum medium (ASM) with peptide amphiphiles (PAs) to engineer functional 3D biofilms of polymicrobial communities. The living ASM/PA material has the capability to fabricate an interkingdom infected lung epithelial model that can be used to study the impact of the antibiotic ciprofloxacin. This study introduces an innovative living material platform based on supramolecular co-assembly and the capability to be liquid-in-liquid bioprinted, offering a fresh concept toward living material design.

This is an open access article under the CC BY license (http://creativecommons.org/licenses/by/4.0/).

Please cite this article in press as: Wu et al., Co-assembling living material as an *in vitro* lung epithelial infection model, Matter (2023), https://doi.org/10.1016/j.matt.2023.10.029

environmental stresses.[8] These properties make biofilms one of the most robust lifestyles in nature,[8] offering unique functionalities with a positive impact, such as decomposing waste[9] and synthesizing high-molecular weight polymers. However, the unique robust properties of biofilms also make them a major hazard that is difficult to treat, such as in the case of antimicrobial resilient biofilms present on hospital surfaces[10] or those infecting patients and showing tolerance of antibiotics.[11] Understanding the underlying properties and recreating the structure of biofilms are critical to tackle these and other biofilm-related problems.[12] A major limitation is the current standard of growing these 3D natural living materials as 2D cultures.

The 3D context of biofilms is critical for the communication between the different microbes within them, ultimately defining the overall biofilm physiology and properties. Aiming to overcome this challenge, Ning et al.[13] and Dubbin et al.[14] fabricated 3D biofilms by bioprinting alginate or bioresin mixed with bacteria, enabling the 3D proliferation of the microorganisms. However, these materials do not recreate the nutritional components of natural biofilms. Particularly, they lack the complex mix of proteins and other macromolecules, like nucleic acids present in real biofluids, which play an important role in the mechanisms of biofilm formation and microbial adherence.[15–17] The use of patient-derived sputum has been key to study the pathobiology of microbial pathogens causing lung disease. This biofluid provides mucins as well as other proteins derived from plasma and products of cell death, such as DNA, which constitute an important nutrient source for pathogenic microorganisms. Mucins have also been associated with gene expression changes and, together with host DNA, enhance biofilm formation by pathogens.

Sputum is a mucous substance secreted by cells in the lower airways of the respiratory tract, comprising structural and nutritional components such as salts, mucin, DNA, and proteins as well as various human cells and polymicrobial communities.[18] The viscous nature of sputum allows it to fight infection by trapping and enabling the killing of bacteria by immune cells. This high viscosity also lowers the diffusion rates impeding the penetration of antibiotics.[19,20] However, in stubborn respiratory infections, bacteria harness the nutrient content of sputum to proliferate, forming 3D biofilms exhibiting a sticky gel-like consistency that plays a critical role in antibiotic tolerance. Artificial sputum medium (ASM) has been used to recreate the environment found in the lung of cystic fibrosis (CF) patients because it includes key nutritional components of native sputum, such as salts, DNA, and key proteins such as mucin,[21] which enable the growth of bacteria found in these patients as biofilms.[22] A real patient sputum is difficult to obtain due to the rigid ethical barrier, and the amount recovered is very low. Therefore, having a way to develop the patient's microbial communities in a matrix similar to the conditions found *in vivo* could circumvent this problem. To build a standard 3D matrix for microorganisms to generate 3D biofilms, we believed that, by triggering ASM into a 3D matrix, it is possible to generate CF-related microorganism 3D biofilms.

Self-assembly, the mechanism by which well-defined nanostructures assemble spontaneously, offers an opportunity to design hydrogels with precise composition and control over molecular display.[23,24] A higher level of complexity can be accessed by self-assembling different types of building blocks,[25] increasing compositional diversity[26,27] and facilitating the emergence of new properties such as structural hierarchy,[28,29] responsive behavior,[30] or the capacity to heal.[31] Multicomponent self-assembly also offers a unique opportunity to engineer complex matrices for cell culture,[26] harnessing the large spectrum of bioactive peptide signals[32] and ECM macromolecules. We have developed methodologies to co-assemble peptides

[1]Plastic and Reconstructive Surgery Department, Wuhan Union Hospital, Tongji Medical College, Huazhong University of Science and Technology, Wuhan 430022, P.R. China

[2]Plastic and Reconstructive Surgery Research Institute, Wuhan Union Hospital, Tongji Medical College, Huazhong University of Science and Technology, Wuhan 430022, P.R. China

[3]Biodiscovery Institute, University of Nottingham, NG7 2RD Nottingham, UK

[4]School of Pharmacy, University of Nottingham, NG7 2RD Nottingham, UK

[5]National Biofilms Innovation Centre, Biodiscovery Institute, University of Nottingham, NG7 2RD Nottingham, UK

[6]School of Life Sciences, University of Nottingham, NG7 2RD Nottingham, UK

[7]Department of Microbiology and Parasitology, Faculty of Biology-CIBUS, Universidad de Santiago de Compostela, 15782 Santiago de Compostela, Spain

[8]Schools of Microbiology and Medicine, University College Cork, and APC Microbiome Ireland, Cork, Ireland

[9]Faculty of Engineering, University of Nottingham, Nottingham NG7 2RD, UK

[10]Hospital of Stomatology, Jilin University, Changchun 130021, P.R. China

[11]Jilin Provincial Key Laboratory of Tooth Development and Bone Remodeling, Jilin University, Changchun 130021, P.R. China

[12]NIHR Nottingham Biomedical Research Centre, University of Nottingham, NG7 2RD Nottingham, UK

[13]These authors contributed equally

[14]Lead contact

*Correspondence: yuanhaowu@hust.edu.cn (Y.W.), a.mata@nottingham.ac.uk (A.M.)

https://doi.org/10.1016/j.matt.2023.10.029

Please cite this article in press as: Wu et al., Co-assembling living material as an *in vitro* lung epithelial infection model, Matter (2023), https://doi.org/10.1016/j.matt.2023.10.029

with macromolecules such as proteins[33,34] and biopolymers,[35,36] including peptide amphiphiles (PAs), with different ECM proteins to grow complex multicellular systems such as cancer[37,38] or bone[36] spheroids. This approach also facilitates incorporation into biofabrication techniques such as 3D printing[39] and expands the complexity of biomaterial design.[40]

Here, we report a self-assembling living material designed to recreate key cellular, nutritional, and structural features of natural 3D biofilms present in sputum of CF patients with respiratory tract infections. The components and properties of real patient sputum are very different from sample to sample. The main goal of our study was to develop a technology that enables practical and relevant investigations of real-life microbial communities for lab testing, which is the ultimate objective and innovative aspect of our work. We use PAs to co-assemble with components present in ASM to generate rich nanofibrous hydrogels emulating natural sputum. The 3D hydrogel environment supports the growth and enable production of 3D biofilms of three major CF pathogens: *Pseudomonas aeruginosa* PAO1-L (Gram-negative), *Staphylococcus aureus* SH1000 (Gram-positive), and *Candida albicans* SC5314 (fungus), individually and as a polymicrobial community of these species. The model was used to co-culture the 3D biofilms with an established lung epithelial (Calu-3) *in vitro* model to build an interkingdom infected lung epithelial model that enabled study of the impact of the antibiotic ciprofloxacin on bacterial biofilms under *in vivo*-like conditions.

In this study, we developed an innovative lung epithelial infection model that integrates supramolecular living materials, biofabrication, and multiple microbial communities. This bottom-up/top-down approach introduces different novelties. First, taking advantage of multi-component self-assembly, we used PA molecules as organizers of ASM components to generate a matrix (i.e., PA-AGD/ASM hydrogel) of composite nanofibers displaying key bioactive peptides (AGD) and macromolecules (e.g., mucin and DNA). This approach offers a novel strategy to engineer complex but reproducible matrices comprising key nutritional signals for bacterial growth. Second, we developed cell-friendly liquid-in-liquid methodologies to trigger PA-ASM co-assembly while directing the assembly into defined hierarchical structures with spatial control. Finally, we demonstrated that the PA-AGD/ASM hydrogel enables 3D biofilm formation and the capacity to rebuild its microstructure as the microorganisms grow, in a manner that is more physiologically relevant compared with commonly used collagen models. By integrating these different factors, we aim to offer a modular platform that can be used to overcome current challenges in the field of living materials and complex interkingdom infection models.

RESULTS

Rationale of the design

PAs were designed to selectively and non-selectively interact with key components of ASM and template their assembly into composite nanofibers to generate rich hydrogels to grow different bacterial communities into 3D biofilms. Given that most ASM components are negatively charged, we designed positively charged PAs to trigger gelation upon co-assembly, incorporating the ASM components within the hydrogel (Figure 1A). The main PA (C_{16}VVVAAAKKKAGD) contained an AGD sequence, a functional motif in fibrinogen[41] (Figures 1B and 1C) that is known to induce biofilm formation.[42] Non-selective electrostatic PA-ASM interactions were assessed using PA-K3 (less charged than PA-AGD) and PA-K4 (more charged than PA-AGD) as controls. The components of ASM (Figure S1A) were tested individually

Please cite this article in press as: Wu et al., Co-assembling living material as an *in vitro* lung epithelial infection model, Matter (2023), https://doi.org/10.1016/j.matt.2023.10.029

A

Name	Sequence	Zeta potential (mV)
PA-K3	$C_{15}H_{31}$CONH-VVVAAA-KKK-NH_2	45.2 ± 0.5
PA-AGD	$C_{15}H_{31}$CONH-VVVAAA-KKKAGD-NH_2	37.3 ± 0.2
PA-K4	$C_{15}H_{31}$CONH-VVVAAA-KKKK-NH_2	31.7 ± 0.2
Artificial sputum medium (ASM)	N/A	-12.3 ± 0.4

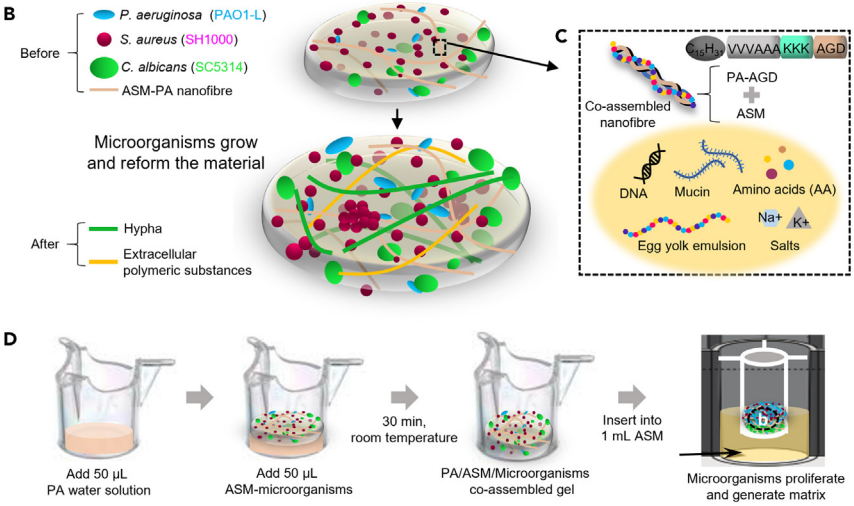

Figure 1. Rationale for co-assembling living material

(A) Table summarizing the key information of the three peptide amphiphile (PA) molecules and artificial sputum medium (ASM) used in the study. The PA-AGD molecule compromises the functional motif AGD from fibrinogen, known to support the growth of biofilms.[42]

(B) Illustration of the components of PA/ASM/microorganism hydrogels designed to generate a physiologically relevant milieu capable of reformation by the growing microorganisms.

(C) Schematic of the PA-ASM co-assembly, depicting the molecular and resulting supramolecular components.

(D) Flowchart of the steps used to prepare and culture the PA/ASM/microorganism hydrogel.

by co-assembly with these three PA sequences into nano- and microstructures. Then, mucin and DNA were found to be the key ASM components to trigger co-assembly with PA-AGD (Figure S1) into hydrogels displaying well-defined fiber nano- and microstructures (Figure S1B). The PA-AGD/ASM hydrogel was used to establish clinically relevant biofilms that are typically present in respiratory tract infections such as those of the CF lung,[43,44] including the pathogens *P. aeruginosa* PAO1-L (PAO1), *S. aureus* SH1000 (SH1000), and *C. albicans* SC5314 (SC5314) (Figures 1B and 1D). Furthermore, we rationalized that these microorganisms would grow and produce EPSs that would continue to interact with the PAs, allowing an evolving PA/ASM microstructure. Finally, an established lung epithelial (Calu-3) *in vitro* model was used to co-culture with the resulting PA/ASM/microorganism living material and mimic an *in vivo* respiratory tract infection scenario.

Characterization of the PA/ASM co-assembly system

Supramolecular characterization of PA/ASM co-assembly

To determine the charge differences between PA-AGD, PA-K3, and PA-K4, zeta potential was first used and revealed that PA-AGD had a zeta potential (37.3 mV) between that of PA-K3 (45.2 mV) and PA-K4 (31.7 mV) (Figure 1A). Then, dynamic light scattering (DLS) measurements were used to estimate the particle size change of PAs before and after co-assembly with ASM. PA-AGD co-assembled with ASM to form

Please cite this article in press as: Wu et al., Co-assembling living material as an *in vitro* lung epithelial infection model, Matter (2023), https://doi.org/10.1016/j.matt.2023.10.029

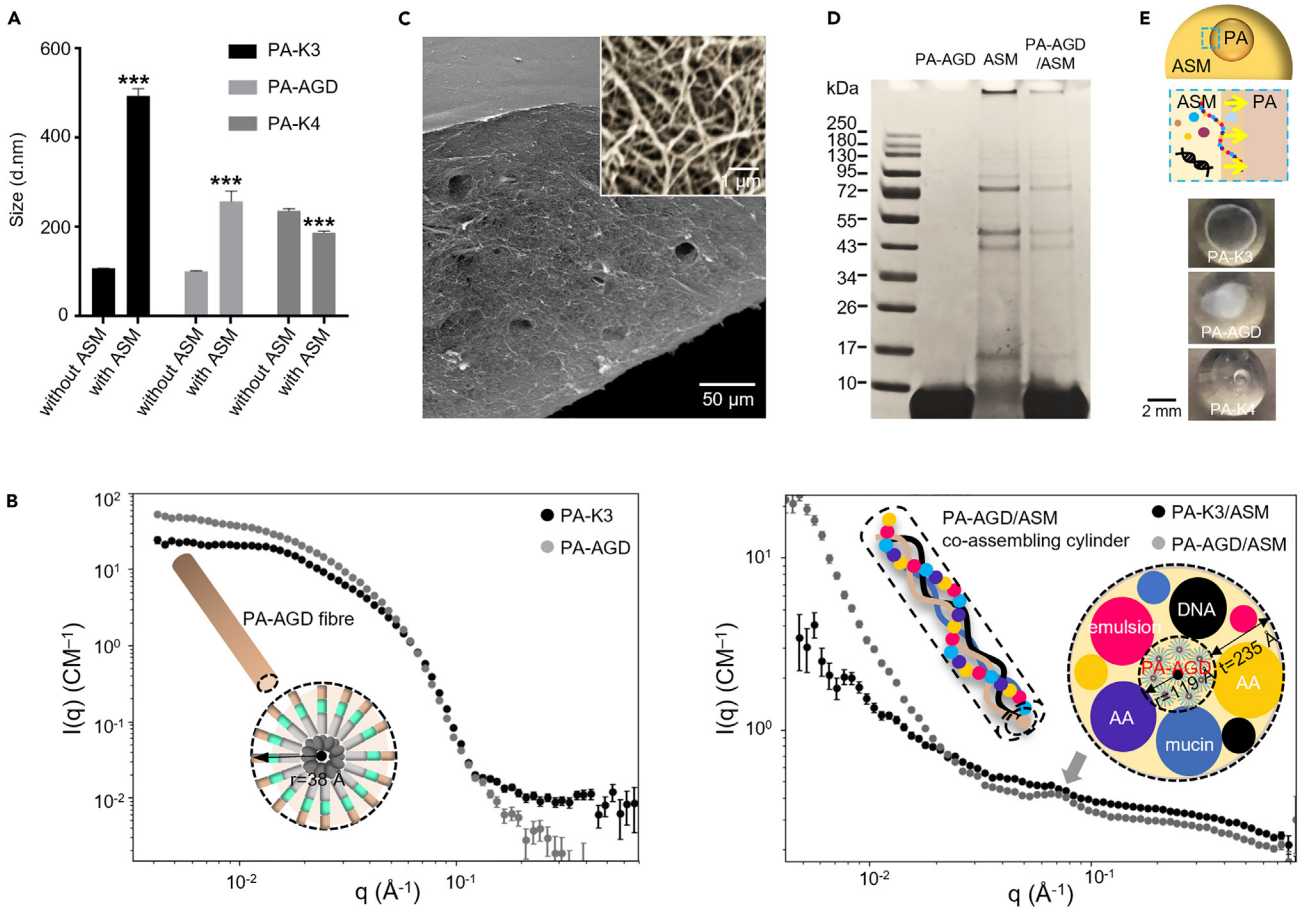

Figure 2. Properties of the co-assembled PA/ASM hydrogel

(A) Dynamic light scattering (DLS) revealing the intermediate size of PA-AGD/ASM co-assemblies compared with PA-K3/ASM and PA-K4/ASM.

(B) Small-angle neutron scattering (SANS) patterns of 38-Å radius PA-AGD-only fibril micelles (left) and PA-AGD/ASM co-assembled nanofibers (right), exhibiting a characteristic scattering peak (gray arrow) associated with a uniform core-shell cylinder complex different from that of the PA-AGD fibrous micelles.

(C) Scanning electron microscopy (SEM) images depicting the homogeneous and fibrous nanostructure (inset) of the PA-AGD/ASM hydrogel.

(D) Sodium dodecyl sulfate–polyacrylamide gel electrophoresis (SDS–PAGE) showing the presence of all ASM components in the PA-AGD/ASM hydrogels.

(E) Illustration showing the components in ASM diffusing into the PA solution at the liquid-liquid interface to generate the gel. Images illustrate the co-assembly when a drop of PA solution is immersed in a larger drop of ASM solution (PA-K3/ASM-membrane, PA-AGD/ASM-hydrogels, PA-K4/ASM-viscous liquid). Error bars present ± SD. *0.01 < p < 0.05, **p < 0.01.

particle of ~260 nm, which were smaller than PA-K3/ASM (~460 nm) but bigger than PA-K4/ASM (~190 nm) (Figure 2A). The particle size of co-assembled structures correlates with the propensity of interactions,[33] suggesting that intermolecular interactions in PA-AGD/ASM are weaker than those in PA-K3/ASM but stronger than those in PA-K4/ASM. These results confirm that electrostatic interactions between PAs and ASM play an important role in their co-assembly.

Nanoscale characterization of PA/ASM co-assembly structures

To investigate the co-assembled PA/ASM nanostructures, we used small-angle neutron scattering (SANS) and found that PA-AGD self-assembled in water into cylindrical nanofibers with a 38-Å radius (Figure 2B, left, gray graph). However, after co-assembly with ASM, PA-AGD/ASM displayed a significant peak around the middle-*q* range (Figure 2B, right, gray arrow), which indicates a uniform co-assembly

Please cite this article in press as: Wu et al., Co-assembling living material as an *in vitro* lung epithelial infection model, Matter (2023), https://doi.org/10.1016/j.matt.2023.10.029

complex. In addition, pronounced scattering appeared at low-*q* in PA-AGD/ASM, which correspond to aggregates with smooth surfaces, further validating a uniform co-assembled hydrogel. By fitting the graph (Figure 2B, right, gray graph), the resulting PA-AGD/ASM nanostructure was interpreted as a core-shell cylindrical nanofiber consisting of a PA-AGD core with a 119-Å radius and an ASM shell 235 Å in thickness (Figures S2 and 2B, right). In addition, PA-K3 controls self-assembly into similar fiber nanostructures as PA-AGD (Figure 2B, left, black graph), but after co-assembly, PA-K3/ASM did not exhibit the distinctive middle-*q* peak observed in PA-AGD/ASM (Figure 2B, right, black graph), indicating lack of uniformity in the co-assembled complex. These results demonstrate that PA-AGD co-assembles with ASM into hydrogels with hierarchically uniform nanofibers.

Microscale characterization of PA/ASM co-assembling structures

To characterize the PA-AGD/ASM co-assemblies at the microscale, scanning electron microscopy (SEM) (Figure 2C) observations first revealed homogeneous nanofibrous networks (Figure 2C, inset) that resemble the classic PA nanofibers. Then, to characterize the composition of these nanofibers and the resulting gels, we used mass spectrometry (MS) and sodium dodecyl sulfate-polyacrylamide gel electrophoresis (SDS-PAGE). MS revealed that PA-AGD and all components of the ASM were incorporated in the co-assembly hydrogel (Figure S3). The SDS-PAGE confirmed this finding by showing that all bands representing the different molecular weights within PA-AGD and the ASM were present in the co-assembly hydrogel (Figure 2D). These results demonstrate that the PAs are able co-assemble with the ASM into nanofibrous ASM-rich hydrogels, opening the possibility to be used as complex but easily assembled 3D microenvironments for cell culture.

Macroscale characterization of PA/ASM co-assembly hydrogels

We then focused on characterizing the co-assembly kinetics and macrostructure properties of PA/ASM hydrogels. To do so, stereoscopic microscopy was first used to investigate the liquid-liquid interface formed when a 5-μL drop of 2% PA water solution was injected into a larger 10-μL drop of ASM (Figure 2E). Upon PA-K3 and ASM co-assembly, an interfacial barrier formed spontaneously and triggered the diffusion of ASM components toward the PA-K3 solution. A similar membranous co-assembly structure and diffusion pattern of macromolecules moving toward a PA solution has been reported previously using elastin-like proteins and PAs.[33] In contrast, when co-assembling PA-AGD with ASM, diffusion led to the formation of a robust 3D hydrogel rather than a 2D membrane (Figure 2E). We hypothesize that a weaker affinity between PA-AGD and ASM (Figure 2A) led to a more permeable interfacial barrier than that of PA-K3/ASM, facilitating the continuous diffusion of macromolecules from the ASM to the PA-AGD solution. This hypothesis was supported by the co-assembly of PA-K4 and ASM, which also led to a looser 3D hydrogel. In this case, PA-K4 and ASM exhibited an even weaker affinity, which may play a key role in the higher permeability of the system (Figures 2A and 2E). Overall, the results demonstrate that PA-AGD can co-assemble with ASM into stable hydrogel macrostructures rich in ASM nutrients that simulate natural sputum.

Engineered living materials of 3D biofilms

Supporting the growth of 3D biofilms as PA-AGD/ASM/microorganism hydrogels

The PA-AGD/ASM hydrogel was then tested to assess its capacity to support the growth of different types of microbial pathogens frequently coexisting in 3D biofilms of CF lung infections. These are the fungus SC5314, the Gram-negative PAO1, and the Gram-positive SH1000. We first focused on assessing the growth of each

Please cite this article in press as: Wu et al., Co-assembling living material as an *in vitro* lung epithelial infection model, Matter (2023), https://doi.org/10.1016/j.matt.2023.10.029

CellPress
OPEN ACCESS

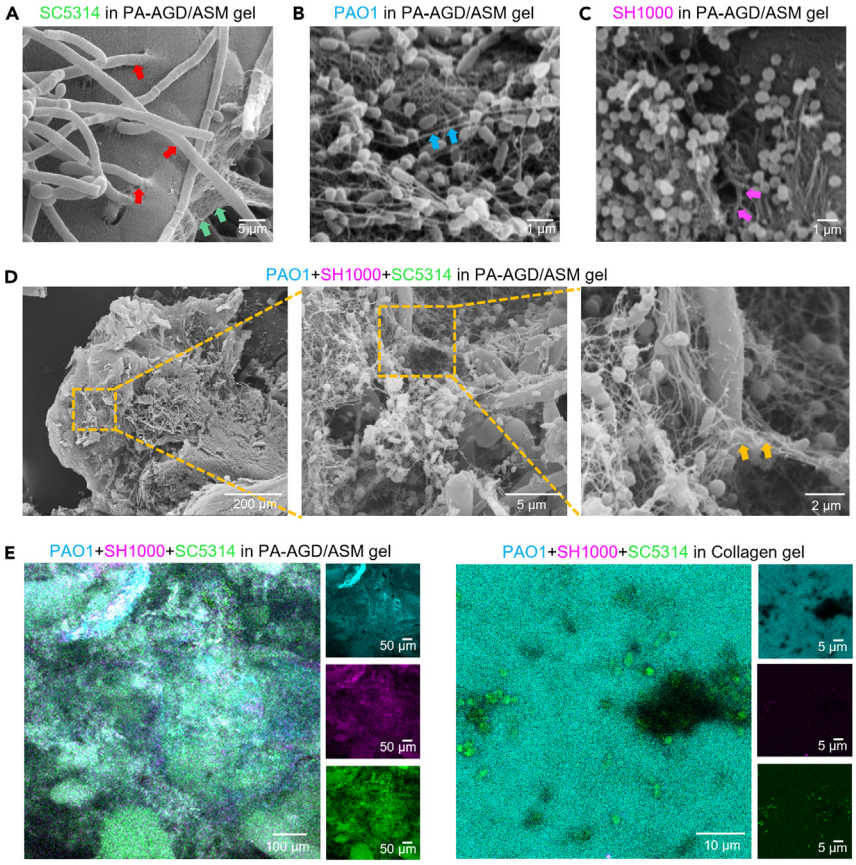

Figure 3. Structure properties of PA/ASM/microorganism hydrogels comprising 3D biofilms

(A–D) SEM images depict 3D biofilms after 24-h culture of (A) A SC5314, (B) PAO1, (C) SH1000, and (D) a community of these 3 species in the PA/ASM hydrogels exhibiting the characteristic matrix microstructures.

(E) Confocal images illustrating 3D biofilms after 24-h culture of the community comprising the 3 species growing within PA/ASM hydrogels (left) in contrast with biofilms growing in the collagen gels (right) exhibiting PAO1 overgrowth. Hyphae, red arrows; nanofibrils, green, cyan, pink, and yellow arrows.

microorganism individually within our co-assembled hydrogel. The specific microorganisms were used at optimized densities (10^3/mL PAO1 , 10^7/mL SH1000 , and 10^6/mL SC5314) and premixed with ASM, enabling their incorporation within the hydrogels upon PA-AGD/ASM co-assembly. All three formed 3D microorganism colonies embedded in EPS within the hydrogels (Figures 3A–3C), with SC5314 bodies producing a dense hyphal network (Figure 3A, red arrow). Also, all three cultures exhibited morphological nanofibril differences compared with those of the PA-AGD/ASM hydrogel in the absence of the microorganisms (Figure 2C, inset). Prior to microorganism culture, the nanofibrils of the PA-AGD/ASM hydrogels were concentrated and coarse (Figure 2C, inset). In contrast, after 24 h of incubation with the microorganisms, the nanofibrils surrounding SC5314 were thin and dense (Figure 3A, green arrow), those of PAO1 were long and thin (Figure 3B, cyan arrow), and those of SH1000 were short and thick (Figure 3C, pink arrow). We speculate that these morphological differences in the nanofibers observed within each of the cultures may result from the PA nanofibers templating the assembly of newly formed EPSs produced by the microorganisms. We believe that this morphology difference results from the growth of different microorganism species, given that the only

Please cite this article in press as: Wu et al., Co-assembling living material as an *in vitro* lung epithelial infection model, Matter (2023), https://doi.org/10.1016/j.matt.2023.10.029

difference between these cultures was the specific species used. The capacity of organisms to remodel the matrix is a characteristic of living materials, a process that was observed within the PA-AGD/ASM hydrogels. These results align with previous findings revealing morphological nanofiber differences upon PA-ECM co-assembly[45] as well as those observed in PA nanofibers before and after ASM co-assembly (Figure 2A).

We then conducted 24-h cultures incorporating all three microbial species. The main challenge of co-culturing polymicrobial communities, including *P. aeruginosa*, is the antagonistic nature of this bacterial pathogen toward other microbial species.[46] Interestingly, we found that the growth of polymicrobial communities within the hypha/nanofibril-rich PA-AGD/ASM hydrogels (Figure 3D, yellow arrow) exhibited colonies of all species and no domination of PAO1 (Figure 3E, left). In contrast, collagen hydrogels were able to support the growth of independent strains for 24 h, which was verified by analyzing the microorganism proliferation by colony-forming unit (CFU) counting (Figure S4). However, polymicrobial cultures grown in collagen gels displayed a dominant growth of PAO1 with only a few SC5314 bodies observed without hyphae (Figure 3E, right). Unlike the PA-AGD/ASM hydrogel, the collagen hydrogel can support the growth of independent strains, but not in the case of polymicrobial cultures at microorganismal densities. We believe that this finding may result from the collagen having a limited capacity to interact with EPS and, consequently, may impose some restrictions on the formation of 3D biofilms by the microorganisms. These results demonstrate that PA-AGD/ASM/microorganism hydrogels support the growth of fungi and bacteria as well as polymicrobial communities capable of remodeling the material's ECM while preventing domination of *P. aeruginosa*.

Engineered *in vitro* infection model integrating 3D biofilms and Calu-3 epithelial cells

Validation of biocompatibility with and toxicity to lung-related cells

Given the living nature of the PA-AGD/ASM/microorganism hydrogels, we then focused on engineering a respiratory tract infection *in vitro* model incorporating lung-relevant cells. For this purpose, we first assessed the biocompatibility of the co-assembling gels using eukaryotic cells to ensure that any potential damage to them would be attributed to the infection. Consequently, lung fibroblast (MRC5) and epithelial (Calu-3) cell lines were used to mimic the natural environment of the native respiratory tract.[47] To demonstrate the biocompatibility of the PA-AGD/ASM hydrogels, these two cell lines were cultured on a porous insert membrane with the co-assembled hydrogels positioned on top. Hyaluronic acid (HA) hydrogels exhibited high biocompatibility when cultured with the MRC5 and Calu-3 cell lines (Figure 4) and, consequently, were used as non-cytotoxic controls. We used a ToxiLight assay to investigate potential cytotoxic effects caused as a result of cell exposure to the PA-AGD/ASM hydrogel. After 24 h of co-culture, cell viability of MRC5 and Calu-3 cells remained greater than 80%, and no significant difference was observed between PA-AGD/ASM hydrogels and HA controls (Figure 4A), demonstrating the biocompatibility of the co-assembly system. Furthermore, PA-AGD/ASM hydrogels were deposited on top of Calu-3 cells and cultured for 10 days. The hydrogels remained stable and were not degraded by the kinetic metabolism of the cells growing directly underneath (Figure 4B). Calu-3 cells exposed to the PA-AGD/ASM hydrogels were stained (Figure 4C) and quantified (Figure 4D) for ZO1 and mucin expression and did not exhibit any disruption of their tight junctions or mucin production compared with those growing in the blank (without the hydrogel on top) or HA control groups. Equally, MRC5 cells stained for F-actin displayed

Please cite this article in press as: Wu et al., Co-assembling living material as an *in vitro* lung epithelial infection model, Matter (2023), https://doi.org/10.1016/j.matt.2023.10.029

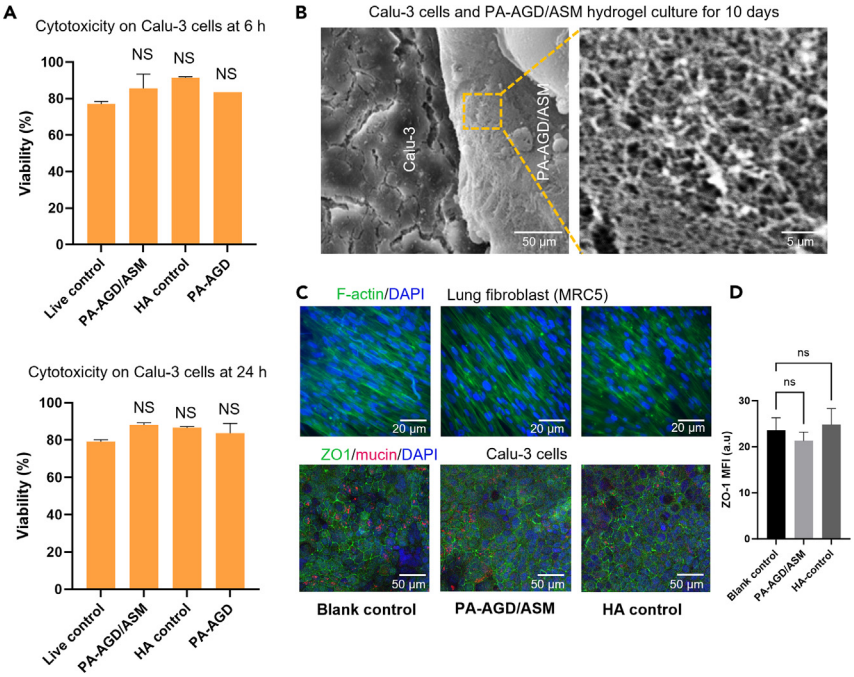

Figure 4. *In vitro* biocompatibility of lung-related eukaryotic cells growing on the PA/ASM hydrogels

(A) ToxiLight relative light unit (RLU) assay illustrating that the PA/ASM hydrogels were not toxic to lung epithelial cells (Calu-3) after 6 h and 24 h of co-culture.

(B) SEM images demonstrating that the PA/ASM hydrogels did not degrade when positioned on top of Calu-3 cells for 10 days of co-culture.

(C) Confocal images showing the similar antibody expression of MRC5 cells (green, F-actin) and Calu-3 cells (green, ZO1; red, mucin) for 10 days in PA/ASM hydrogel as well as blank control and positive control (HA hydrogel) groups.

(D) Quantification of ZO1 (tight junction barrier) expressed as mean fluorescence intensity (MFI). No significant difference in expression is shown between controls and PA-ASM hydrogels. Error bars present ±SD. *0.01 < p < 0.05, **p < 0.01.

filamentous actin, indicating an undisrupted cytoskeleton. These results demonstrate the biocompatibility of PA-AGD/ASM hydrogels and their potential to serve as *in vitro* models of the respiratory tract.

Co-assembling the PA-AGD/ASM/microorganism hydrogel with the Calu-3 cell in vitro epithelial model

To demonstrate the functionality of our hydrogel system to recreate key features of a respiratory tract infection, 5 μL of PA-AGD/ASM/microorganism hydrogels simulating infected sputum were positioned on the surface of a Calu-3 cell *in vitro* epithelial model (Figure 5A). We prepared PA-AGD/ASM/microorganism hydrogels using PAO1, and *trans*-epithelial electric resistance (TEER) measurements were conducted every 10 min to assess the moment when tight junctions between Calu-3 cells begin to be destroyed. TEER measurements revealed a drop as acute infection developed from ~900 Ω cm^2 to ~600 Ω cm^2 after 30 min of culturing PA-AGD/ASM/PAO1 hydrogels on top of Calu-3 cells, indicating that the PA-AGD/ASM/PAO1 hydrogels began to disrupt the tight junctions between Calu-3 cells. This result was supported by a LIVE/DEAD assay revealing that most cells were dead by 6 h, and almost no cells were alive after 24 h (Figure 5B). These findings suggest that antibiotics may be applied within 30 min after incorporation of the PA-AGD/ASM/PAO1 hydrogel to avoid any weakening of the tight junction barrier.

Please cite this article in press as: Wu et al., Co-assembling living material as an *in vitro* lung epithelial infection model, Matter (2023), https://doi.org/10.1016/j.matt.2023.10.029

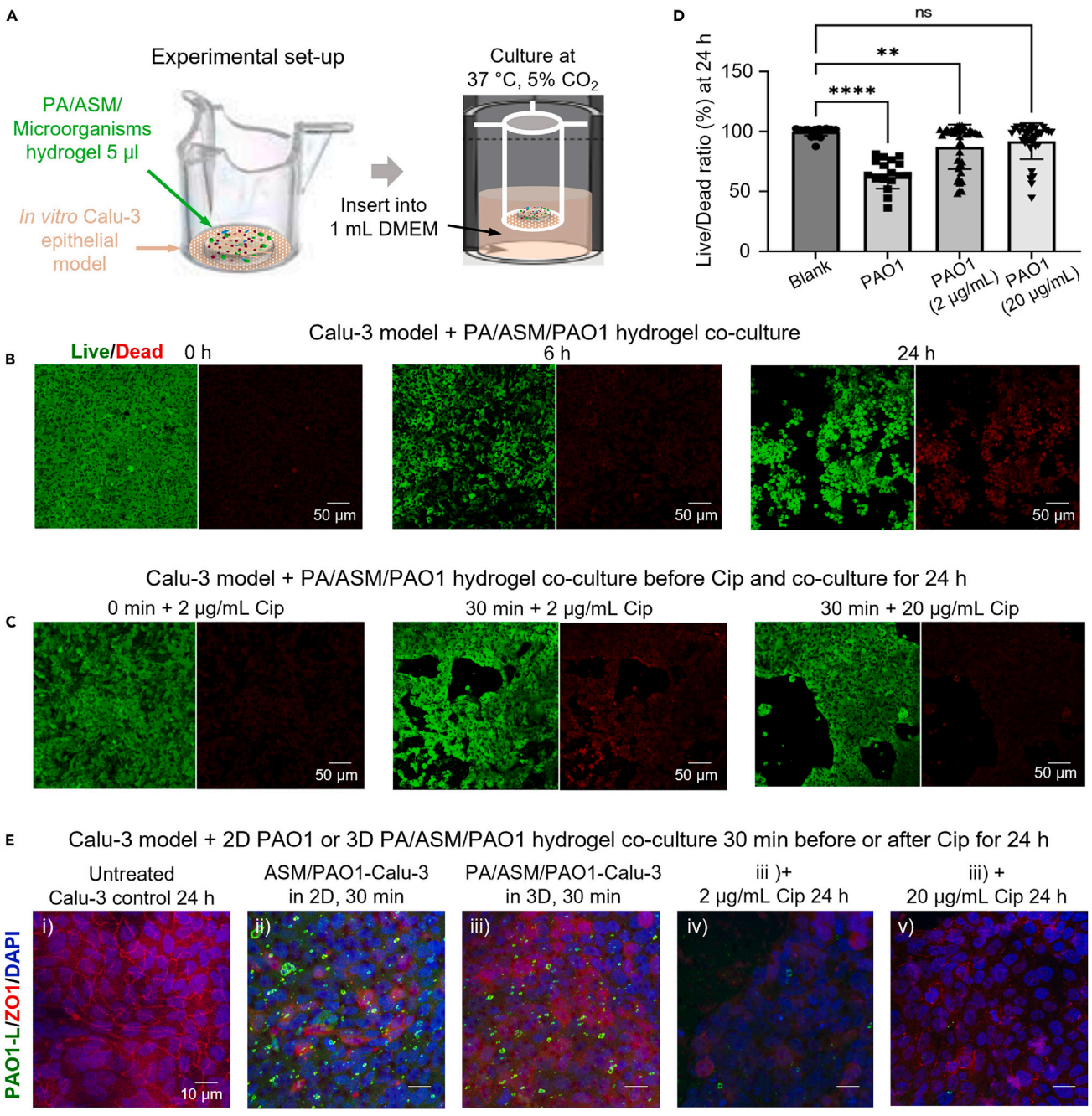

Figure 5. PA/ASM/PAO1 hydrogels co-cultured with the Calu-3 *in vitro* model to test infection

(A) Illustration of the experimental setup consisting of PA/ASM/PAO1 hydrogels being positioned on top of Calu-3 cells to build the co-culture model.

(B) LIVE/DEAD (green/red) assay illustrating the biovalidation of Calu-3 cells. The Calu-3 cells began to detach from the insert surface at 6 h, and all died in 24 h when cultured with the hydrogels.

(C and D) With different co-culture periods (0 min, 30 min) of Calu-3 and PA/ASM/PAO1 hydrogels before addition of the antibiotic ciprofloxacin (Cip), the different doses of Cip, with (D) the corresponding image assay indicating that 2 µg/mL was enough for the survival of the Calu-3 cells when applied at the beginning of co-culture, and 20 µg/mL Cip was necessary when applied after 30-min co-culture.

(E) Immunostaining indicating (i) untreated Calu-3 cells as a blank control expressing the continuous tight junctions (ZO1), (ii) Calu-3 cells cultured with PAO1 as 2D biofilms losing most ZO1 in 30 min, (iii) while kept more ZO1 by culturing with PA/ASM/PAO1 hydrogel where PAO1 as 3D biofilms (iv) 2 µg/mL Cip was not enough to keep ZO1, and (v) 20 µg/mL Cip was necessary to protect ZO1 between Calu-3 cells. Error bars present ± SD.

*$0.01 < p < 0.05$, **$p < 0.01$.

Please cite this article in press as: Wu et al., Co-assembling living material as an *in vitro* lung epithelial infection model, Matter (2023), https://doi.org/10.1016/j.matt.2023.10.029

CellPress
OPEN ACCESS

PA-AGD/ASM/PAO1-Calu-3 in-vitro-*infected epithelial model response to ciprofloxacin*

3D biofilms present in sputum lead to high antibiotic tolerance within the respiratory tract.[48,49] Thus, an ideal *in vitro*-infected epithelial model should be able to simulate antibiotic tolerance. To assess this within our PA-AGD/ASM/PAO1-Calu-3 *in vitro* model, the broad-spectrum antibiotic ciprofloxacin (Cip), which is used extensively for treatment of respiratory infections, was tested by supplementing 1 mL Dulbecco's modified Eagle's medium (DMEM) with the antibiotic in 24-well plates holding the inserts for culture (Figure 5A). First, Cip was applied to PA-AGD/ASM/PAO1 hydrogels without Calu-3 cells to estimate the antibiotic tolerance of 3D biofilms growing within the hydrogels (Figure 1D; Figure S5). CFU counting and fluorescence microscope observations revealed that the hydrogel incorporating the 3D biofilms of 3 strains could tolerate up to 2 μg/mL of Cip (10× the minimum inhibitory concentration (MIC) of planktonic *P. aeruginosa* cells[50]) (Figure S5). After the tight junctions of Calu-3 cells were disrupted by the microorganisms presented in PA-AGD/ASM/microorganism hydrogels, the antibiotic was able to penetrate the hydrogels and kill relevant microbes. Thus, the effect of the antibiotic was similar to that caused by PA-AGD/ASM/microorganism hydrogels without Calu-3 cells. With this dose of Cip in mind, we then assessed whether Cip treatment would allow survival of Calu-3 cells after exposure to polymicrobial hydrogels. Two concentrations of Cip (2 and 20 μg/mL) were used and delivered using two different methods: (1) PA-AGD/ASM/PAO1 hydrogel and Cip applied together to the Calu-3 *in vitro* epithelial model and (2) first co-culture of the PA-AGD/ASM/PAO1 hydrogel and the Calu-3 *in vitro* epithelial model for 30 min to destroy the tight junctions and application of Cip. A LIVE/DEAD assay was conducted after 24-h co-culture of the hydrogels and Calu-3 *in vitro* epithelial models for all groups.

For method (1), 2 μg/mL of Cip was enough to protect Calu-3 cells from being killed by PAO1, and no significant differences were observed between the blank control of the Calu-3 *in vitro* epithelial model and the PA-AGD/ASM/PAO1 hydrogels. For method (2), higher concentrations of Cip (20 μg/mL) were needed to protect the Calu-3 cells (Figures 5C and 5D). These results indicate that delivery method (2) allows higher antibiotic tolerance of the microbial communities, which is more clinically relevant. To validate this finding, immunostaining was used to characterize tight junctions (ZO1, shown in red) and a self-fluorescent PAO1 (shown in green) to visualize the PA-AGD/ASM/PAO1 hydrogel. After 30-min culture combining the hydrogel and the Calu-3 *in vitro* epithelial model, the tight junctions of ZO1 were partially lost (Figure 5Eiii). In contrast, the control 2D biofilm generated by culturing PAO1 in liquid ASM for 24 h exhibited more damaged tight junctions (Figure 5Eii), which might result from the free migration of PAO1 cells. These findings again confirm that the invasive properties of 2D and 3D biofilms are different and, consequently, demonstrate the importance of recreating 3D biofilms to better mimic the natural scenario. The confocal images of more ZO1 in 20 μg/mL (Figure 5Ev) than in 2 μg/mL (Figure 5Eiv) demonstrates that the 3D biofilms within the PA-AGD/ASM/PAO1-Calu-3 *in vitro* model were able to tolerate at least 2 μg/mL of Cip. However, 2 μg/mL is the highest concentration 3D biofilms in PA-AGD/ASM/PAO1 hydrogel can tolerate without Calu-3 cells. Furthermore, this result indicates that 20 μg/mL of Cip is the dose needed to protect tight junctions of the Calu-3 *in vitro* epithelial model from PAO1 infection.

Engineered PA-AGD/ASM/PAO1+SH1000+SC5314 polymicrobial community/Calu-3 with a 3D biofilm to establish an in-vitro-*infected lung epithelial model*

A respiratory tract infection normally contains a community of multiple microbial species. To engineer an *in vitro*-infected lung epithelial model, we co-cultured PA/ASM/PAO1-mTurq+SH1000-YFP+SC5314-yCherry (all strains were fluorescently labeled)

Please cite this article in press as: Wu et al., Co-assembling living material as an *in vitro* lung epithelial infection model, Matter (2023), https://doi.org/10.1016/j.matt.2023.10.029

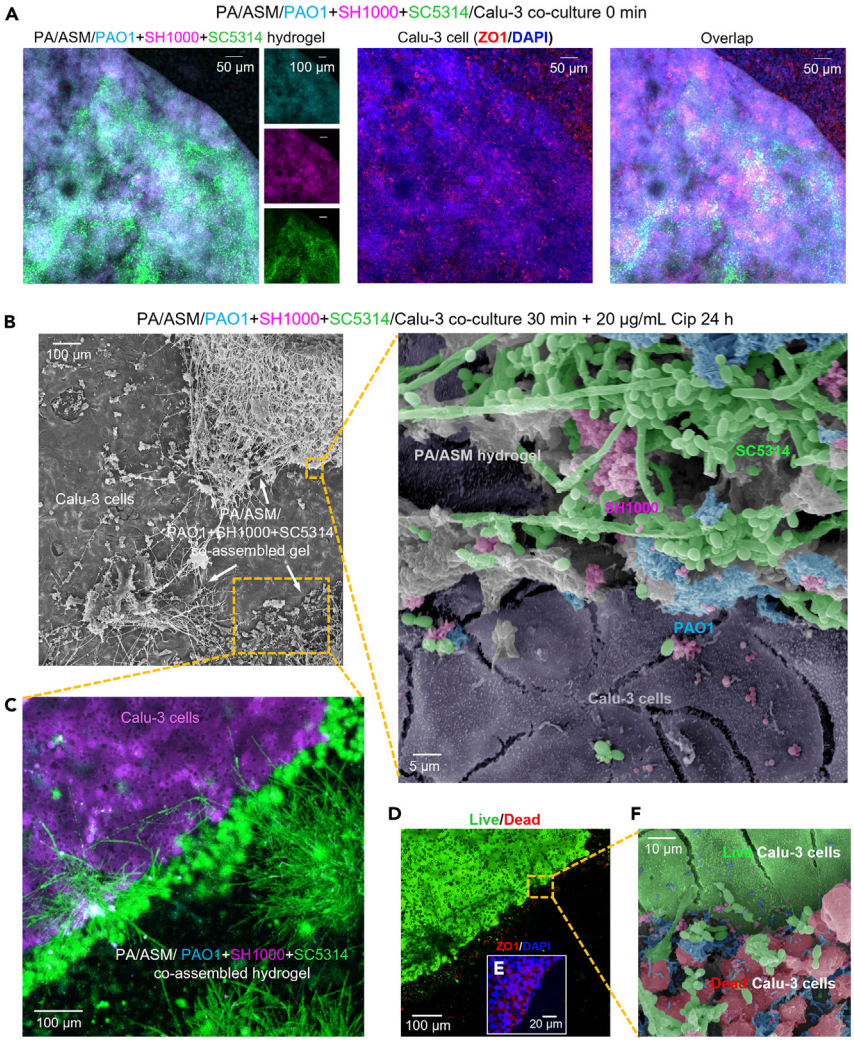

Figure 6. PA-AGD/ASM/PAO1+SH1000+SC5314 polymicrobial community/Calu-3 to build an infected lung epithelial *in vitro* model

(A) Confocal image illustrating the polymicrobial 3D biofilms within the hydrogels on top of Calu-3 cells expressing tight junction antibodies (ZO1).

(B) SEM image demonstrating the *in vitro*-infected lung epithelial model integrating the polymicrobial 3D biofilms and the Calu-3 epithelial cells.

(C–E) Immunostaining showing an interface between Calu-3 cells and the polymicrobial 3D biofilms (C) and LIVE/DEAD assay for the same view (D), showing that Calu-3 cells at the interface were dead, while those on the Calu-3 cell side (left) were alive with integrated tight conjunctions (E, inset).

(F) SEM image illustrating the interface consisting of dead Calu-3 cells and 3 species of microorganisms.

hydrogels on top of the Calu-3 *in vitro* epithelial model (Figure 6A). To establish an interkingdom *in vitro* model, 20 μg/mL Cip was applied by adding it to 1 mL DMEM in 24-well plates outside of the insert (Figure 5A). SEM (Figures 6B and 6F), confocal imaging of the fluorescent strains (Figures 6C and 6E), and LIVE/DEAD assays (Figure 6D) were conducted to investigate the growth of the polymicrobial community and Calu-3 *in vitro* model. SEM imaging confirmed that the microorganisms growing within the 3D biofilms were located on top of the layer of Calu-3 epithelial cells (Figure 6B, left). Higher magnification observations illustrated the healthy morphologies of each of

Please cite this article in press as: Wu et al., Co-assembling living material as an *in vitro* lung epithelial infection model, Matter (2023), https://doi.org/10.1016/j.matt.2023.10.029

CellPress
OPEN ACCESS

the microbial species, PA/ASM hydrogel, and Calu-3 cells (Figure 6B, right). Prior to SEM examination, confocal imaging showed that the self-fluorescent strains were clearly present and growing over Calu-3 cells within the hydrogel (Figure 6C). Furthermore, LIVE/DEAD assays confirmed that the Calu-3 cells were alive (Figure 6D), and immunostaining demonstrated the integrity of their tight junctions (Figure 6E). In addition, the boundary area was observed at the interface between the microbial community and the Calu-3 epithelial cells. Furthermore, LIVE/DEAD assays evidenced that more dead cells were at the boundary (Figure 6D), which are likely the result of the cytotoxicity of the microbial community (Figure 6F). These results demonstrate that the *in vitro*-infected lung epithelial model is able to support the growth of polymicrobial communities and eukaryotic cells and represents a realistic scenario of respiratory tract infection with antibiotic tolerance.

Biofabrication properties

We developed a living micro-organism material with the capacity to be integrated with eukaryotic cells to engineer an *in vitro*-infected lung epithelial model. The mechanical properties are another critical parameter to consider when designing living materials and 3D printing processes.[6,51] In this regard, viscosity is the most critical parameter for assessing the mechanical properties of infected sputum from respiratory tract-infected patients. Therefore, viscosity tests were conducted and revealed that the value (~10 mPa s) of PA-AGD/ASM co-assembly hydrogels was similar to that of real sputum from CF patients with a mild infection[52] (Figure 7A). The capacity to incorporate such living materials within additive manufacturing would allow the fabrication of different types of models enabling spatial control of biofilm structure and geometry over multiple length scales. Taking advantage of PA-ASM co-assembly and liquid-in-liquid printing (Figure 7B), we integrated the PA-ASM co-assembly system with extrusion-based (Figure 7C) and inkjet-based printing to demonstrate the viability of this approach. By extruding PA-AGD solution into ASM, self-supported and well-defined filaments were fabricated into intricate single- or multilayered geometries (Figure 7C; Video S1). Furthermore, by spraying PA-AGD solution into ASM, nanoscale particles were also fabricated (Figure 7D). In addition to versatility of fabrication, the ASM-PA system was applied by incorporation with a zigzag polydimethylsiloxane (PDMS) template fabricated using standard protocols.[53] The 5-μm-wide channels were filled with PA-AGD solution first, and ASM with PAO1 was added on top to co-assemble the gel in the channel. After 24-h culture, the LIVE/DEAD assay indicated that PAO1 grew well inside the 3D hydrogel (Figure 7E).

Increased levels of the bacterial intracellular signal c-di-guanosine monophosphate (GMP) has been associated with biofilm formation.[54] Therefore, a c-di-GMP-dependent transcriptional fusion, P*cdrA-gfp*^{S},[55] able to report on the levels of this signal, was used to monitor biofilm formation activity in the PA gel by the PAO1 strain harboring this fusion and constitutively expressing the fluorescent protein mCherry. The modified PAO1 with ASM was premixed with the prepared hydrogels in a star-shaped PDMS concave template. After 24 h incubation, GFP fluorescence was detected in the 3D hydrogels, showing the production of c-di-GMP and, hence, reporting biofilm formation (Figure 7F). These results demonstrate that, by taking advantage of the liquid-to-gel transition of the co-assembly system, high-resolution (~5 μm) biofabrication with 3D biofilms was feasible.

DISCUSSION

We demonstrated the possibility to co-assemble PAs and the complex biofluid ASM into a hierarchical homogeneous hydrogel designed to display key functional

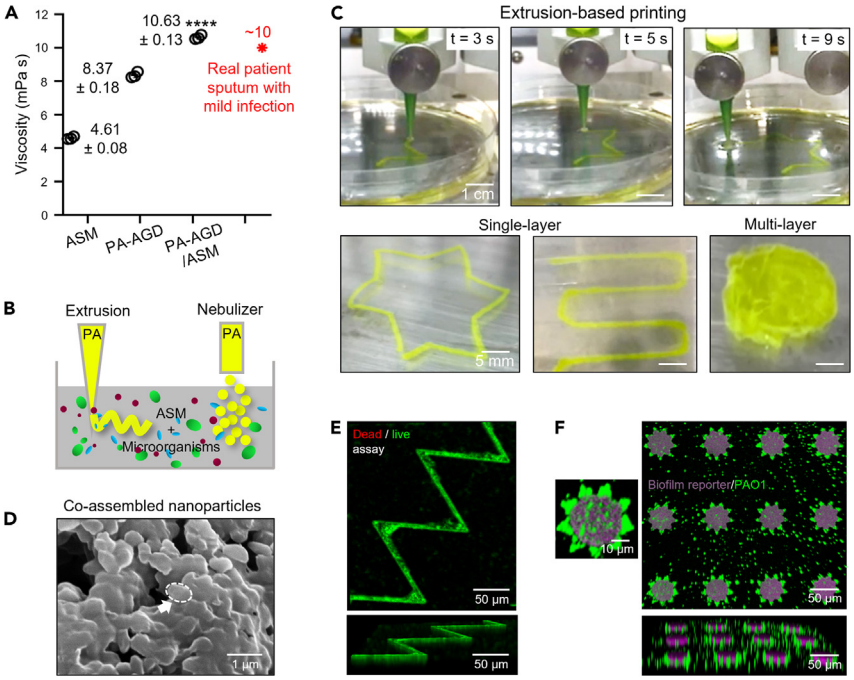

Figure 7. Biofabrication of the PA/ASM system

(A) Graph indicating that the viscosity of PA-AGD/ASM hydrogel was higher than that of individual PA-AGD or ASM and similar to the sputum of CF patients with mild infection.[49]

(B) Illustration of the approach to combine the PA/ASM co-assembly system with extrusion-based and inkjet-based 3D printing.

(C) Time-lapse images demonstrating the rapid PA/ASM printing using an extrusion-based 3D printer to generate single- or multi-layer structures with high fidelity.

(D) SEM image depicting the homogeneous PA/ASM nanoparticle structures (white arrow) with 300-nm diameter generated by a nebulizer, which was similar to the structure generated by an inkjet-based 3D printer but with higher resolution.

(E) LIVE/DEAD assay demonstrating the biovalidation of a biofabricated PA/ASM/PAO1 system incorporated within a 5-μm-wide zigzag channel template.

(F) Confocal images illustrating the modified PAO1 producing 3D biofilms (green, PAO1; purple, biofilms). Error bars present ± SD. *0.01 < p < 0.05, **p < 0.01.

peptides and transform ASM components into structural building blocks. This material can support the growth of 3D biofilms of different strains of microorganisms, including individual Gram-positive and Gram-negative bacteria and fungi as well as polymicrobial communities made of these. In this way, the multicomponent self-assembling material offers a more physiologically relevant milieu capable of promoting more realistic polymicrobial growth. Furthermore, we demonstrated how the microorganisms can reform the nanostructure of the co-assembling material as they grow, suggesting that the PA/ASM/microorganism hydrogel behaves as a living material. In addition, we illustrated the capability to integrate the PA/ASM/microorganism hydrogel with a Calu-3 *in vitro* model to build an infected *in vitro* epithelial model of the respiratory tract and tested it with different concentrations of the antibiotic Cip. Altogether, we developed a "biocooperative" platform that harnesses a complex biofluid (ASM) to engineer a living material that can recreate features of 3D biofilms and build an interkingdom *in vitro* model of polymicrobial communities and living tissue cells. A main novelty of our study is the integration of (1) molecular and supramolecular design, (2) bioengineering of reproducible hierarchical materials with complex composition, (3) growth of multiple microbial communities, and (4) practical biofabrication methods. Our study has reached the

Please cite this article in press as: Wu et al., Co-assembling living material as an *in vitro* lung epithelial infection model, Matter (2023), https://doi.org/10.1016/j.matt.2023.10.029

major goal of improving the complexity of the matrix to recreate 3D biofilms and developed methodologies to do so in a reproducible and controllable manner. However, it is important to mention that the differences present in sputum samples between different patients should not be ignored. In this case, the next step of our study will focus on developing customized co-assembling living systems that enable the use of real sputum samples.

EXPERIMENTAL PROCEDURES

Resource availability

Lead contact

Further information and requests for resources should be directed to the lead contact, Alvaro Mata (a.mata@nottingham.ac.uk).

Materials availability

This study did not generate new unique reagents.

Data and code availability

All experimental and theoretical data are available upon reasonable request from the lead contact.

Materials

PA-K3 (purity, 99.1%), PA-AGD (purity, 98.7%), and PA-K4 (purity, 98.3%) were designed as reported previously[56] and purchased from Biomatik (ON, Canada). ASM was prepared in house following the recipe reported by Kirchner et al.[57]

Microbial strains and culture conditions

The PAO1 and SH1000 strains were routinely propagated in lysogeny broth (LB; Oxoid, Cambridge, UK) for 16 h at 37°C with shaking at 250 rpm, and SC5314 was propagated in yeast peptone dextrose (YPD) broth (Oxoid) for 16 h at 30°C with shaking at 200 rpm. For biofilm growth, 16-h planktonic cultures of PAO1, SH1000, and SC5314 were washed twice by centrifugation (10,000 × *g*) and resuspended in 1× phosphate-buffered saline (PBS), and cell numbers were adjusted to different CFUs/mL, respectively, in ASM. For selective isolation of microbes, *Pseudomonas* isolation agar (PIA; Oxoid) and mannitol salt agar (MSA; Oxoid) were utilized. To prevent growth of bacteria during the enumeration of SC5314, tetracycline (Sigma-Aldrich, Haverhill, UK) was added to a final concentration of 125 μg/mL to Sabouraud dextrose agar (SAB; Oxoid). To prevent growth of SC5314 during MSA enumeration, nystatin (Sigma-Aldrich) was added to a final concentration of 8 μg/mL.

Hydrogel biofilm model setup

50 μL of a 2 wt % PA-AGD solution in water was added to a 24-well insert (83.3925.500, Sarstedt, Newton, NC, USA). Microorganisms, including PAO1, SH1000, and SC5314, were premixed with ASM at various densities for different targets, as described in the under Microbial strains and culture conditions. Microorganisms were prepared in 50 μL of ASM and mixed with the PA-AGD solution in the insert to form a standard hydrogel. This hydrogel was cultured in a 24-well plate with 1 mL ASM at 37°C. Antibiotic treatments were applied via the outer ASM in the microwell plate.

Zeta potential (ζ)

To illustrate the co-assembly mechanism of the ASM-PA systems, the ζ of Pas were measured on a Zetasizer (Nano-ZS ZEN 3600, Malvern Instruments, Worcestershire, UK) at room temperature. The concentration of PAs used for the measurements was

0.1 wt %. The pH values of solutions were adjusted to be equal to pHs of PA solutions at 2 wt % using 1 M HCl and 1 M NH_4OH. The samples were equilibrated for 30 min at room temperature prior to measurement of their ζ.

DLS

DLS was performed to measure the particle sizes of PAs and ASM-PAs. The PAs were dissolved separately in MilliQ water at a concentration of 0.1%, and ASM was diluted using MilliQ water. The two solutions were mixed at a 1:1 ratio, and the particle sizes were measured using a Zetasizer (Nano-ZS ZEN 3600, Malvern Instruments). Samples were equilibrated for 10 min at room temperature before measurements.

SEM

The microstructures of ASM-PA hydrogels with or without microorganisms were first fixed with 4% paraformaldehyde (PFA) for 30 min and then dehydrated using increasing concentrations of ethanol water solvents (70%, 90%, 96%, and 100%). All samples were subjected to a critical point dryer (EM CPD300, Leica, Wetzlar, Germany) prior to imaging. The SEM micrographs were captured on an Inspect Q600 (FEI, Eindhoven, the Netherlands) after sputter coating with gold (10 nm thick).

SDS-PAGE and gel digestion

For SDS-PAGE analysis, PA, ASM, and ASM-PA samples were pipetted up and down to break hydrogel matrices, vortexed for 1 min to allow homogenization, and diluted 10-fold in PBS. Before SDS-PAGE gel loading, samples were prepared by mixing 15 μL of PA, ASM, and ASM-PA solution with 7 μL Bolt 4× Lithium dodecyl sulfate (LDS) loading buffer and 3 μL Bolt 4× reducing agent (Thermo Fisher Scientific, Carlsbad, CA, USA). Solutions were heated at 80°C for 5 min on a heating block (HB120-S, Scilogex, USA). After heating, 25 μL of each sample was loaded in pre-cast NuPAGE 4%–12% BisTris mini protein gels mounted on Invitrogen mini gel tanks (Thermo Fisher Scientific). Samples were run alongside 5 μL of pre-stained protein ladder PageRuler Plus (range, 10–250 kDa, Thermo Fisher Scientific). To visualize protein bands, NuPAGE gels were run for 1 h at 120 V using NuPAGE MES SDS running buffer (Thermo Fisher Scientific), stained overnight with InstantBlue (Expedeon, Germany), and imaged using a compact scanner (CanoScan LiDE 220, Japan). For gel digestion, NuPAGE gels were run for 5 min at 120 V using NuPAGE MES SDS running buffer (Thermo Fisher Scientific). Gel bands were stained overnight at 4°C with InstantBlue, and staining solution was replaced with deionized water. Bands of interest were excised from the gel, dehydrated using acetonitrile followed by vacuum centrifugation, reduced with 10 mM dithiothreitol, and alkylated with 55 mM iodoacetamide. Gel pieces were then washed twice with 25 mM ammonium bicarbonate followed by acetonitrile before trypsin digestion overnight at 37°C.

Liquid chromatography-tandem MS (LC-MS/MS)

Digested samples were analyzed by LC-MS/MS using UltiMate 3000 Rapid Separation LC (RSLC; Dionex, CA, USA) coupled to a Q Exactive HF-X Hybrid Quadrupole-Orbitrap Mass Spectrometer (Thermo Fisher Scientific). Mobile phase A was 0.1% formic acid in water, and mobile phase B was 0.1% formic acid in acetonitrile, and the column used was a 75 mm × 250 μm i.d. 1.7 mM charged surface hybrid (CSH) C18 analytical column (Waters, Wilmslow, UK). A 1-μL aliquot of the sample was transferred to a 5-μl loop and loaded onto the column at a flow rate of 300 nL/min for 5 min at 5% B. The loop was then taken out of line, and the flow was reduced from 300 nL/min to 200 nL/min in 0.5 min. Peptides were separated using a gradient that went from 5% to 18% B in 34.5 min, then from 18% to 27% B in 8 min, and finally from 27% B to 60% B in 1 min. The column was washed at 60% B for 3 min

Please cite this article in press as: Wu et al., Co-assembling living material as an *in vitro* lung epithelial infection model, Matter (2023), https://doi.org/10.1016/j.matt.2023.10.029

before re-equilibration to 5% B in 1 min. At 55 min, the flow was increased to 300 nL/min until the end of the run at 60 min. MS data were acquired in a data-directed manner for 60 min in positive mode. Peptides were selected automatically for fragmentation by data-dependent analysis on the basis of the top 12 peptides with *m/z* between 300 and 1,750 Th and a charge state of 2, 3, or 4 with dynamic exclusion set at 15 s. The MS resolution was set at 120,000 with an AGC target of 3e6 and a maximum fill time set at 20 ms. The MS2 resolution was set to 30,000 with an AGC target of 2e5, a maximum fill time of 45 ms, an isolation window of 1.3 Th, and a collision energy of 28.

LC-MS/MS data analysis

Data produced were searched using Mascot (Matrix Science, Chicago, IL, US), against the Swissprot and Trembl databases with the taxonomy of *Sus scrofa*. Data were validated using Scaffold (Proteome Software, Portland, OR, USA). From the raw data containing identified proteins and numbers of matched peptides, only proteins containing at least 4 unique peptides were accepted. Processed data were used to compare protein compositions of PA, ASM, and ASM-PA samples.

SANS

The PAs were dissolved in D_2O with 2 wt %, and PA (2 wt %)-ASM gels (50% D_2O/50% H_2O) were prepared for measuring. SANS measurements were performed on the fixed-geometry, time-of-flight ZOOM diffractometer (ISIS Neutron and Muon Source, Oxfordshire, UK). A white beam of radiation with neutron wavelengths spanning 2.2–10 Å was enabled access to Q [$Q = 4\pi\sin(\theta/2)/\lambda$] range of 0.004–0.4 $Å^{-1}$ with a fixed-sample detector distance of 4.1 m. Solutions (0.4 mL) of individual components were contained in 1-mm-path-length UV spectrophotometer-grade quartz cuvettes (Hellman), while the composite peptide-drug gel was prepared in a demountable 1-mm-path-length cuvettes. The cuvettes were mounted in aluminum holders on top of an enclosed, computer-controlled sample chamber at 25°C. Time taken for each measurement was approximately 30 min. All scattering data were normalized for the sample transmission, the backgrounds was corrected using a quartz cell filled with D_2O, and the linearity and efficiency of the detector response were corrected using the instrument-specific software.

3D printing

3D printing was performed on a commercial extrusion printer (Cellink, MA, USA). Print designs were created using commercial software (Autodesk, San Francisco, CA, USA) and sliced with the free software Slic3r (https://slic3r.org/). PA-AGD (2 wt %) was dyed with thioflavin T (0.5 μL/mL) and extruded into a bath of ASM through a 22G nozzle at a printhead movement speed of 40 mm/s.

Viscosity test

A four-channel liquid-handling apparatus (Microlab STARlet, Hamilton Robotics, Reno, NV, USA) was used to characterize the viscosity of PA-AGD (2 wt %), ASM, and PA-AGD (2 wt %)/ASM gel. This method has been developed to simultaneously characterize viscosities of multiple samples in a high-throughput manner.[58] The results have proven to be highly accurate in comparison with conventional viscosity measurement methods such as using an oscillatory rheometer. 300 μL of each sample was added to a 96-well polypropylene plate containing 1-mL wells (260252, Thermo Fisher Scientific), which was placed in a heating module at 25°C. Three replicates were tested for each sample. Samples were aspirated into 300-μL pipettes (235902, CO-RE non-filter tips, Hamilton Robotics) attached to channels on the test head at 10 μL for 15 s. Submerge depth was set at 2 mm

Please cite this article in press as: Wu et al., Co-assembling living material as an *in vitro* lung epithelial infection model, Matter (2023), https://doi.org/10.1016/j.matt.2023.10.029

below the liquid surface. The testing generated real-time pressure data, which were subsequently used to calculate viscosities of tested samples using a self-developed MATLAB program.

Imaging of the biofilm model

Microbial localization was determined by utilizing fluorescent protein (FP)-expressing strains grown in appropriate media with the following antimicrobial selection: PAO1 mTurquoise2 (125 μg/mL tetracycline [TC]), SH1000 pTK005 YFP (40 μg/mL chloramphenicol [CM]), and *C. albicans* CAF2 yCherry. To assess the viability of the microbial population in the polymicrobial biofilms, wild-type strains (no FP) were stained with the LIVE/DEAD BacLight Bacterial Viability Kit (L7007, Fisher Scientific, Loughborugh, UK) according to the manufacturer's instructions. Following staining, biofilms were rinsed with sterile water and imaged using an LSM 700 laser-scanning confocal microscope (CLSM; Carl Zeiss, Wetzlar, Germany).

Calu-3 cell culture and gel application

Calu-3 cells (ATCC, HTB-55) were cultured in Eagle's Minimum Essential Medium (MEM) (Sigma-Aldrich) supplemented with 10% fetal bovine serum (FBS), 1% penicillin/streptomycin, 1% GlutaMAX, 1% sodium pyruvate, and 1% non-essential amino acids until 80% confluent. Cells were trypsinized using trypLE (Gibco), and 4×10^5 cells/cm^2 were seeded onto the apical side of a Polyester (PET) Transwell membrane with 5-μm pore size (Sarstedt) for 4–5 days at 37°C in 5% CO_2. Cells were then subjected to an air-liquid interface for a further 3–4 days until a monolayer formed. 10 μL PA-AGD/ASM gel with or without microorganisms was applied directly to the surface of the monolayer of Calu-3 cells.

Cell viability and cytotoxicity testing

Calu-3 cells were assessed for viability using LIVE/DEAD stain (Fisher Scientific) following exposure to gels for 6 and 24 h. In brief, ethidium homodimer-1 and calcein AM were mixed at a 1:4 ratio in PBS and applied to cells for 20 min at 37°C. Cells were viewed using an Etaluma Lumascope 720 microscope. Cytotoxicity tests were carried out using a ToxiLight non-destructive bioassay kit (Lonza, Basel, Switzerland) according to the manufacturer's instructions. Luminescence was read at 1-s intervals on a GloMax Discover microplate reader (Promega, Southampton, UK).

Immunofluorescence staining

Immunofluorescence staining was performed to determine whether addition of the gels had any detrimental effect on Calu-3 cell barrier integrity. Membranes with cells were fixed in 4% formaldehyde solution (VWR Chemicals, Singapore, Singapore) for 15 min and rinsed twice in PBS. Cells were permeabilized with Triton X-100 (0.5%, Thermo Fisher Scientific) for 5 min, followed by 3 5-min rinses with PBS Tween 20 (0.2%). Non-specific binding was blocked by incubating cells in PBS with goat serum (10%, Thermo Fisher Scientific) for 1 h at room temperature. Primary antibody staining was undertaken using rabbit anti-human ZO-1 (1:100, Thermo Fisher Scientific) and incubation overnight at 4°C. Cells were rinsed with PBS Tween 20 (0.2%) prior to goat anti-rabbit immunoglobulin G (IgG; H+L) Alexa Fluor 488 secondary antibody staining (1:200, Thermo Fisher Scientific) for 1 h at room temperature, followed by counterstaining with DAPI. Membranes were mounted using Prolong Gold Antifade reagent (Fisher Scientific) and viewed using an LSM 700 CLSM (Carl Zeiss).

SUPPLEMENTAL INFORMATION

Supplemental information can be found online at https://doi.org/10.1016/j.matt.2023.10.029.

ACKNOWLEDGMENTS

The work was supported by the ERC Proof-of-Concept grant (NOVACHIP), the Medical Research Council (UK Regenerative Medicine Platform Acellular/Smart Materials 3D Architecture, MR/R015651/1), the NIHR Nottingham Biomedical Research Centre, CF Trust, CF Foundation (grant "PIPE-CF" Ref. SRC 022), and European Union's Horizon 2020 Research and Innovation programme under grant agreement 760921(PANBioRA). The work (Y.W.) was supported by the National Natural Science Foundation of China (82302837), Queen Mary University of London, and Huazhong University of Science and Technology - Strategic Partnership Research Fund (5001530148). M.R. is supported by the Maria Zambrano Program from the Spanish Ministry of Universities. National Biofilms Innovation Centre (NBIC), which is an Innovation and Knowledge Center, is funded by the Biotechnology and Biological Sciences Research Council, Innovate UK and Hartree Centre (awards BB/R012415/1 and BB/X002950/1). The SANS experiment at the ISIS was allocated beamtime under experiment number RB2010335 and collected on ZOOM. We thank Dr. Diego Alba Venero from STFC, UKRI for supporting the study of SANS. The 3D printing and materials screening was funded by the Engineering and Physical Sciences Research Council under research grant EP/N024818/1 ("Formulation for 3D Printing: Creating a Plug and Play Platform for a Disruptive UK Industry").

AUTHOR CONTRIBUTIONS

Y.W., M.C., and A.M. conceived the project. Y.W. and M.R. carried out the experiments. A.M., Y.W., M.C., and J.S. supervised the study. S.N.R., L.F., A.M.G., W.B., H.S., and J.S. performed biological characterization. I.W. and L.M.P. performed the collagen-ASM experiments. S.F. supported the project by preparing the ASM. C.L. conducted the LC-MS/MS and analyzed the data. J.H., Z.Z., and R.D.W. conducted the mechanical characterization and 3D printing.

DECLARATION OF INTERESTS

The authors declare no competing interests.

Received: June 12, 2023
Revised: September 7, 2023
Accepted: October 24, 2023
Published: November 21, 2023

REFERENCES

1. Liu, A.P., Appel, E.A., Ashby, P.D., Baker, B.M., Franco, E., Gu, L., Haynes, K., Joshi, N.S., Kloxin, A.M., Kouwer, P.H.J., et al. (2022). The living interface between synthetic biology and biomaterial design. Nat. Mater. *21*, 390–397. https://doi.org/10.1038/s41563-022-01231-3.

2. Rodrigo-Navarro, A., Sankaran, S., Dalby, M.J., del Campo, A., and Salmeron-Sanchez, M. (2021). Engineered living biomaterials. Nat. Rev. Mater. *6*, 1175–1190. https://doi.org/10.1038/s41578-021-00350-8.

3. Mimee, M., Nadeau, P., Hayward, A., Carim, S., Flanagan, S., Jerger, L., Collins, J., McDonnell, S., Swartwout, R., Citorik, R.J., et al. (2018). An ingestible bacterial-electronic system to monitor gastrointestinal health. Science *360*, 915–918. https://doi.org/10.1126/science.aas9315.

4. Johnston, T.G., Yuan, S.F., Wagner, J.M., Yi, X., Saha, A., Smith, P., Nelson, A., and Alper, H.S. (2020). Compartmentalized microbes and co-cultures in hydrogels for on-demand bioproduction and preservation. Nat. Commun. *11*, 563. https://doi.org/10.1038/s41467-020-14371-4.

5. Gantenbein, S., Colucci, E., Käch, J., Trachsel, E., Coulter, F.B., Rühs, P.A., Masania, K., and Studart, A.R. (2023). Three-dimensional printing of mycelium hydrogels into living complex materials. Nat. Mater. *22*, 128–134. https://doi.org/10.1038/s41563-022-01429-5.

6. Liu, X., Yuk, H., Lin, S., Parada, G.A., Tang, T.C., Tham, E., de la Fuente-Nunez, C., Lu, T.K., and Zhao, X. (2018). 3D Printing of Living Responsive Materials and Devices. Adv. Mater. *30*. https://doi.org/10.1002/adma.201704821.

7. Flemming, H.C., and Wingender, J. (2010). The biofilm matrix. Nat. Rev. Microbiol. *8*, 623–633. https://doi.org/10.1038/nrmicro2415.

8. Lieleg, O., Caldara, M., Baumgärtel, R., and Ribbeck, K. (2011). Mechanical robustness of Pseudomonas aeruginosa biofilms. Soft Matter *7*, 3307–3314. https://doi.org/10.1039/c0sm01467b.

9. Sehar, S., Naz, I., Sehar, S., and Naz, I. (2016). Role of the Biofilms in Wastewater Treatment. In Microbial Biofilms - Importance and Applications, D. Dhanasekaran and N. Thajuddin, eds., pp. 121–145.

10. Costa, D.M., Johani, K., Melo, D.S., Lopes, L.K.O., Lopes Lima, L.K.O., Tipple, A.F.V., Hu, H., and Vickery, K. (2019). Biofilm contamination of high-touched surfaces in intensive care units: epidemiology and

Please cite this article in press as: Wu et al., Co-assembling living material as an *in vitro* lung epithelial infection model, Matter (2023), https://doi.org/10.1016/j.matt.2023.10.029

potential impacts. Lett. Appl. Microbiol. *68*, 269–276. https://doi.org/10.1111/lam.13127.

11. Deva, A.K., Adams, W.P., Jr., and Vickery, K. (2013). The role of bacterial biofilms in device-associated infection. Plast. Reconstr. Surg. *132*, 1319–1328. https://doi.org/10.1097/PRS.0b013e3182a3c105.

12. Flemming, H.C., Wingender, J., Szewzyk, U., Steinberg, P., Rice, S.A., and Kjelleberg, S. (2016). Biofilms: an emergent form of bacterial life. Nat. Rev. Microbiol. *14*, 563–575. https://doi.org/10.1038/nrmicro.2016.94.

13. Ning, E., Turnbull, G., Clarke, J., Picard, F., Riches, P., Vendrell, M., Graham, D., Wark, A.W., Faulds, K., and Shu, W. (2019). 3D bioprinting of mature bacterial biofilms for antimicrobial resistance drug testing. Biofabrication *11*, 045018. https://doi.org/10.1088/1758-5090/ab37a0.

14. Dubbin, K., Dong, Z., Park, D.M., Alvarado, J., Su, J., Wasson, E., Robertson, C., Jackson, J., Bose, A., Moya, M.L., et al. (2021). Projection Microstereolithographic Microbial Bioprinting for Engineered Biofilms. Nano Lett. *21*, 1352–1359. https://doi.org/10.1021/acs.nanolett.0c04100.

15. Alhede, M., Alhede, M., Qvortrup, K., Kragh, K.N., Jensen, P.Ø., Stewart, P.S., and Bjarnsholt, T. (2020). The origin of extracellular DNA in bacterial biofilm infections in vivo. Pathog. Dis. *78*, ftaa018. https://doi.org/10.1093/femspd/ftaa018.

16. Moormeier, D.E., and Bayles, K.W. (2017). Staphylococcus aureus biofilm: a complex developmental organism. Mol. Microbiol. *104*, 365–376. https://doi.org/10.1111/mmi.13634.

17. Landry, R.M., An, D., Hupp, J.T., Singh, P.K., and Parsek, M.R. (2006). Mucin-Pseudomonas aeruginosa interactions promote biofilm formation and antibiotic resistance. Mol. Microbiol. *59*, 142–151. https://doi.org/10.1111/j.1365-2958.2005.04941.x.

18. Alguire, P.C. (1990). Tonometry. Clinical Methods: The History, Physical, and Laboratory Examinations, 3rd edition, H.K. Walker, W. Dallas Hall, and J. Willis Hurst, MD, eds., pp. 581–584.

19. Wilton, M., Charron-Mazenod, L., Moore, R., and Lewenza, S. (2016). Extracellular DNA Acidifies Biofilms and Induces Aminoglycoside Resistance in Pseudomonas aeruginosa. Antimicrob. Agents Chemother. *60*, 544–553. https://doi.org/10.1128/AAC.01650-15.

20. Russo, P., Stigliani, M., Prota, L., Auriemma, G., Crescenzi, C., Porta, A., and Aquino, R.P. (2013). Gentamicin and leucine inhalable powder: what about antipseudomonal activity and permeation through cystic fibrosis mucus? Int. J. Pharm. *440*, 250–255. https://doi.org/10.1016/j.ijpharm.2012.05.077.

21. Turner, K.H., Wessel, A.K., Palmer, G.C., Murray, J.L., and Whiteley, M. (2015). Essential genome of Pseudomonas aeruginosa in cystic fibrosis sputum. Proc. Natl. Acad. Sci. USA *112*, 4110–4115. https://doi.org/10.1073/pnas.1419677112.

22. Wang, J., Lory, S., Ramphal, R., and Jin, S. (1996). Isolation and characterization of Pseudomonas aeruginosa genes inducible by respiratory mucus derived from cystic fibrosis patients. Mol. Microbiol. *22*, 1005–1012. https://doi.org/10.1046/j.1365-2958.1996.01533.x.

23. Aida, T., Meijer, E.W., and Stupp, S.I. (2012). Functional supramolecular polymers. Science *335*, 813–817. https://doi.org/10.1126/science.1205962.

24. Levin, A., Hakala, T.A., Schnaider, L., Bernardes, G.J.L., Gazit, E., and Knowles, T.P.J. (2020). Biomimetic peptide self-assembly for functional materials. Nat. Rev. Chem *4*, 615–634. https://doi.org/10.1038/s41570-020-0215-y.

25. Okesola, B.O., and Mata, A. (2018). Multicomponent self-assembly as a tool to harness new properties from peptides and proteins in material design. Chem. Soc. Rev. *47*, 3721–3736. https://doi.org/10.1039/c8cs00121a.

26. Collier, J.H., Rudra, J.S., Gasiorowski, J.Z., and Jung, J.P. (2010). Multi-component extracellular matrices based on peptide self-assembly. Chem. Soc. Rev. *39*, 3413–3424. https://doi.org/10.1039/b914337h.

27. Xu, C., Martin, N., Li, M., and Mann, S. (2022). Living material assembly of bacteriogenic protocells. Nature *609*, 1029–1037. https://doi.org/10.1038/s41586-022-05223-w.

28. Marshall, L.J., Wallace, M., Mahmoudi, N., Ciccone, G., Wilson, C., Vassalli, M., and Adams, D.J. (2023). Hierarchical Composite Self-Sorted Supramolecular Gel Noodles. Adv. Mater. *35*, e2211277. https://doi.org/10.1002/adma.202211277.

29. Wu, Y., Okesola, B.O., Xu, J., Korotkin, I., Berardo, A., Corridori, I., di Brocchetti, F.L.P., Kanczler, J., Feng, J., Li, W., et al. (2020). Disordered protein-graphene oxide co-assembly and supramolecular biofabrication of functional fluidic devices. Nat. Commun. *11*, 1182. https://doi.org/10.1038/s41467-020-14716-z.

30. Freeman, R., Han, M., Álvarez, Z., Lewis, J.A., Wester, J.R., Stephanopoulos, N., McClendon, M.T., Lynsky, C., Godbe, J.M., Sangji, H., et al. (2018). Reversible self-assembly of superstructured networks. Science *362*, 808–813. https://doi.org/10.1126/science.aat6141.

31. Okesola, B.O., Mendoza-Martinez, A.K., Cidonio, G., Derkus, B., Boccorh, D.K., Osuna de la Peña, D., Elsharkawy, S., Wu, Y., Dawson, J.I., Wark, A.W., et al. (2021). De Novo Design of Functional Coassembling Organic-Inorganic Hydrogels for Hierarchical Mineralization and Neovascularization. ACS Nano *15*, 11202–11217. https://doi.org/10.1021/acsnano.0c09814.

32. Ligorio, C., and Mata, A. (2023). Synthetic extracellular matrices with function-encoding peptides. Nat. Rev. Bioeng. *1*, 518–536. https://doi.org/10.1038/s44222-023-00055-3.

33. Inostroza-Brito, K.E., Collin, E., Siton-Mendelson, O., Smith, K.H., Monge-Marcet, A., Ferreira, D.S., Rodríguez, R.P., Alonso, M., Rodríguez-Cabello, J.C., Reis, R.L., et al. (2015). Co-assembly, spatiotemporal control and morphogenesis of a hybrid protein-peptide system. Nat. Chem. *7*, 897–904. https://doi.org/10.1038/nchem.2349.

34. Majkowska, A., Inostroza-Brito, K.E., Gonzalez, M., Redondo-Gómez, C., Rice, A., Rodriguez-Cabello, J.C., Del Rio Hernandez, A.E., and Mata, A. (2023). Peptide-Protein Coassemblies into Hierarchical and Bioactive Tubular Membranes. Biomacromolecules *24*, 4419–4429. https://doi.org/10.1021/acs.biomac.2c01095.

35. Ajovalasit, A., Redondo-Gómez, C., Sabatino, M.A., Okesola, B.O., Braun, K., Mata, A., and Dispenza, C. (2021). Carboxylated-xyloglucan and peptide amphiphile co-assembly in wound healing. Regen. Biomater. *8*, rbab040. https://doi.org/10.1093/rb/rbab040.

36. Derkus, B., Okesola, B.O., Barrett, D.W., D'Este, M., Chowdhury, T.T., Eglin, D., and Mata, A. (2020). Multicomponent hydrogels for the formation of vascularized bone-like constructs in vitro. Acta Biomater. *109*, 82–94. https://doi.org/10.1016/j.actbio.2020.03.025.

37. Hedegaard, C.L., Redondo-Gómez, C., Tan, B.Y., Ng, K.W., Loessner, D., and Mata, A. (2020). Peptide-protein coassembling matrices as a biomimetic 3D model of ovarian cancer. Sci. Adv. *6*, eabb3298. https://doi.org/10.1126/sciadv.abb3298.

38. Osuna de la Peña, D., Trabulo, S.M.D., Collin, E., Liu, Y., Sharma, S., Tatari, M., Behrens, D., Erkan, M., Lawlor, R.T., Scarpa, A., et al. (2021). Bioengineered 3D models of human pancreatic cancer recapitulate in vivo tumour biology. Nat. Commun. *12*, 5623. https://doi.org/10.1038/s41467-021-25921-9.

39. Wu, Y., Fortunato, G.M., Okesola, B.O., Brocchetti, F.L.P.D., Suntornnond, R., Connelly, J., De Maria, C., Rodriguez-Cabello, J.C., Vozzi, G., Wang, W., and Mata, A. (2021). An interfacial self-assembling bioink for the manufacturing of capillary-like structures with tuneable and anisotropic permeability. Biofabrication *13*, 035027. https://doi.org/10.1088/1758-5090/abe4c3.

40. Azevedo, H.S., and Mata, A. (2022). Embracing complexity in biomaterials design. Biomater. Biosyst. *6*, 100039. https://doi.org/10.1016/j.bbiosy.2022.100039.

41. Zhang, Y., Qiu, Y., Blanchard, A.T., Chang, Y., Brockman, J.M., Ma, V.P.Y., Lam, W.A., and Salaita, K. (2018). Platelet integrins exhibit anisotropic mechanosensing and harness piconewton forces to mediate platelet aggregation. Proc. Natl. Acad. Sci. USA *115*, 325–330. https://doi.org/10.1073/pnas.1710828115.

42. Bonifait, L., Grignon, L., and Grenier, D. (2008). Fibrinogen induces biofilm formation by Streptococcus suis and enhances its antibiotic resistance. Appl. Environ. Microbiol. *74*, 4969–4972. https://doi.org/10.1128/AEM.00558-08.

43. Fourie, R., Ells, R., Swart, C.W., Sebolai, O.M., Albertyn, J., and Pohl, C.H. (2016). Candida albicans and Pseudomonas aeruginosa Interaction, with Focus on the Role of Eicosanoids. Front. Physiol. *7*, 64. https://doi.org/10.3389/fphys.2016.00064.

44. Biswas, L., and Götz, F. (2021). Molecular Mechanisms of Staphylococcus and Pseudomonas Interactions in Cystic Fibrosis. Front. Cell. Infect. Microbiol. *11*, 824042. https://doi.org/10.3389/fcimb.2021.824042.

Please cite this article in press as: Wu et al., Co-assembling living material as an *in vitro* lung epithelial infection model, Matter (2023), https://doi.org/10.1016/j.matt.2023.10.029

45. Hedegaard, C.L., Collin, E.C., Redondo-Gómez, C., Nguyen, L.T., Ng, K.W., Castrejón-Pita, A.A., and Mata, A. (2018). Hydrodynamically guided hierarchical self-assembly of peptide–protein bioinks. Adv. Funct. Mater. *28*, 1703716. https://doi.org/10.1002/adfm.201703716.

46. Quinn, R.A., Whiteson, K., Lim, Y.W., Zhao, J., Conrad, D., LiPuma, J.J., Rohwer, F., and Widder, S. (2016). Ecological networking of cystic fibrosis lung infections. NPJ Biofilms Microbiomes *2*, 4. https://doi.org/10.1038/s41522-016-0002-1.

47. Harrington, H., Cato, P., Salazar, F., Wilkinson, M., Knox, A., Haycock, J.W., Rose, F., Aylott, J.W., and Ghaemmaghami, A.M. (2014). Immunocompetent 3D model of human upper airway for disease modeling and in vitro drug evaluation. Mol. Pharm. *11*, 2082–2091. https://doi.org/10.1021/mp5000295.

48. Müller, L., Murgia, X., Siebenbürger, L., Börger, C., Schwarzkopf, K., Sewald, K., Häussler, S., Braun, A., Lehr, C.M., Hittinger, M., and Wronski, S. (2018). Human airway mucus alters susceptibility of Pseudomonas aeruginosa biofilms to tobramycin, but not colistin. J. Antimicrob. Chemother. *73*, 2762–2769. https://doi.org/10.1093/jac/dky241.

49. Van den Bossche, S., De Broe, E., Coenye, T., Van Braeckel, E., and Crabbé, A. (2021). The cystic fibrosis lung microenvironment alters antibiotic activity: causes and effects. Eur. Respir. Rev. *30*, 210055. https://doi.org/10.1183/16000617.0055-2021.

50. Singh, N., Romero, M., Travanut, A., Monteiro, P.F., Jordana-Lluch, E., Hardie, K.R., Williams, P., Alexander, M.R., and Alexander, C. (2019). Dual bioresponsive antibiotic and quorum sensing inhibitor combination nanoparticles for treatment of Pseudomonas aeruginosa biofilms in vitro and ex vivo. Biomater. Sci. *7*, 4099–4111. https://doi.org/10.1039/c9bm00773c.

51. Nguyen, P.Q., Courchesne, N.M.D., Duraj-Thatte, A., Praveschotinunt, P., and Joshi, N.S. (2018). Engineered Living Materials: Prospects and Challenges for Using Biological Systems to Direct the Assembly of Smart Materials. Adv. Mater. *30*, e1704847. https://doi.org/10.1002/adma.201704847.

52. Tomaiuolo, G., Rusciano, G., Caserta, S., Carciati, A., Carnovale, V., Abete, P., Sasso, A., and Guido, S. (2014). A new method to improve the clinical evaluation of cystic fibrosis patients by mucus viscoelastic properties. PLoS One *9*, e82297. https://doi.org/10.1371/journal.pone.0082297.

53. Mata, A., Boehm, C., Fleischman, A.J., Muschler, G.F., and Roy, S. (2007). Connective tissue progenitor cell growth characteristics on textured substrates. Int. J. Nanomed. *2*, 389–406. https://doi.org/10.2147/IJN.S2.3.389.

54. Hengge, R. (2009). Principles of c-di-GMP signalling in bacteria. Nat. Rev. Microbiol. *7*, 263–273. https://doi.org/10.1038/nrmicro2109.

55. Rybtke, M.T., Borlee, B.R., Murakami, K., Irie, Y., Hentzer, M., Nielsen, T.E., Givskov, M., Parsek, M.R., and Tolker-Nielsen, T. (2012). Fluorescence-based reporter for gauging cyclic di-GMP levels in Pseudomonas aeruginosa. Appl. Environ. Microbiol. *78*, 5060–5069. https://doi.org/10.1128/AEM.00414-12.

56. Mata, A., Palmer, L., Tejeda-Montes, E., and Stupp, S.I. (2012). Design of biomolecules for nanoengineered biomaterials for regenerative medicine. Methods Mol. Biol. *811*, 39–49. https://doi.org/10.1007/978-1-61779-388-2_3.

57. Kirchner, S., Fothergill, J.L., Wright, E.A., James, C.E., Mowat, E., and Winstanley, C. (2012). Use of artificial sputum medium to test antibiotic efficacy against Pseudomonas aeruginosa in conditions more relevant to the cystic fibrosis lung. J. Vis. Exp. *64*, e3857. https://doi.org/10.3791/3857.

58. Zhou, Z., Ruiz Cantu, L., Chen, X., Alexander, M.R., Roberts, C.J., Hague, R., Tuck, C., Irvine, D., and Wildman, R. (2019). High-throughput characterization of fluid properties to predict droplet ejection for three-dimensional inkjet printing formulations. Addit. Manuf. *29*, 100792. https://doi.org/10.1016/j.addma.2019.100792.